Malaysian Journal of Mathematical Sciences 19(4): 1417–1436 (2025)
https://doi.org/10.47836/mjms.19.4.13

Malaysian Journal of Mathematical Sciences

Journal homepage: https://mjms.upm.edu.my

Separation Points Analysis on Unsteady MHD Mixed Convective Heat Transfer Past A Sphere in Casson Fluid

Jefri, N. N. N. [1] and Ali, A. * [1]

[1]*Department of Mathematical Sciences, Faculty of Science, Universiti Teknologi Malaysia, 81310 Skudai, Johor, Malaysia*

E-mail: anati@utm.my
**Corresponding author*

Received: 26 March 2025
Accepted: 9 June 2025

Abstract

This study extends prior work on magnetohydrodynamic (MHD) mixed convective heat transfer in Casson fluids by investigating unsteady flow past a sphere, focusing on the rarely explored phenomenon of flow reversal. The Casson model, which captures a blood-like non-Newtonian behavior, makes the study relevant to biomedical and engineering applications. Minimizing flow reversal is crucial for improving flow stability, reducing energy loss, and enhancing transport efficiency. The governing equations are solved using the Keller box method, implemented via a MATLAB algorithm. Flow reversal is analyzed through graphical representations of velocity and temperature profiles, with particular attention to the effects of magnetic field strength, mixed convection, and the Casson parameter. This study is the first to report the effect of the magnetic field on flow reversal in unsteady Casson fluid flow past a rigid sphere. Results show that the magnetic field parameter reduces the momentum boundary layer thickness, effectively minimizing flow reversal. This novel finding has practical implications in applications such as improving drug delivery by regulating blood flow in arteries and optimizing thermal management in electronic cooling systems around spherical components in aerospace and industrial designs.

Keywords: MHD; mixed convective; Casson; sphere.

1 Introduction

The flow of fluid past a sphere is a complex phenomenon that is influenced by various factors such as the fluid properties, sphere characteristics, and external factors. This type of geometry is closely related to the reversal of the flow past a sphere. The reversal of fluid flow occurs when the boundary layer flow detaches from the surface of the sphere, leading to a distinct wake pattern. The flow reversal can be detected by analyzing the streamlines and flow velocities [31]. The characteristics of a blunt surface and sharp corners lead to the flow separation (flow reversal) around a sphere, which has obtained the greatest attention in engineering applications, especially in construction, mechanics, offshore, and wind power [16]. Therefore, the study of separation regions over spheres is crucial for engineering applications such as aerodynamic design, drag reduction, and optimization of flow control in various industries, including automotive and aerospace, where understanding flow patterns enhances performance and efficiency [33]. Numerous engineering applications benefit from the flow of a sphere, including sports balls, combustion engines, the movement of silt in streams, water conveying, pneumatic machinery, and the production of food and chemicals [1]. In the outcome, the researcher needs to look into the separation zones because of their widespread use in fluid flow past a sphere.

Due to its relevance in various industrial processes such as the production of glass fibers, plastic films, crystal growth, and paper processing, as well as the need for advanced modeling in engineering applications, the non-Newtonian model for fluid flow is used in this study [5]. The Casson model, a form of non-Newtonian fluid with unique properties, is utilized to examine the non-Newtonian behavior of blood flow, considered as the base fluid [7]. This research on Casson fluids holds great potential for medical applications, especially in refining drug delivery methods through blood vessels to treat cardiovascular ailments [32]. This type of non-Newtonian fluid is distinguished by its yield stress and distinct rheological properties, which make it very useful in a variety of industrial and biological applications [23]. This fluid model is critical for studying the flow behavior of materials that exhibit both elastic and viscous properties, such as blood and certain polymer solutions [28]. Casson fluid is used in endoscopy to diagnose abnormalities in internal organs which is essential to maintain the slope of the pressure fluctuation in an artery [11]. Yanala et al. [34] reported that Casson fluid is widely used in pharmaceutical manufacturing, integration of biological fluids like synovial fluids with China clay. As a result, Subbarao et al. [30] and Yuan et al. [35] investigated the flow past a sphere in Casson fluid. In summary, the Casson fluid flow model is very useful in biomedical engineering for drug delivery and other engineering fields. This Casson model is well suited for biomedical studies because it captures both the yield stress and shear-thinning behaviour of blood [8]. Then, the rigid sphere, as used in this study, serves not only as a simplified geometric model but also closely mimics the behavior of individual blood cells or hemoglobin aggregates in circulation, offering valuable insights into the dynamics of blood flow, oxygen transport, and potential blockages in biological systems.

In this study, the MHD effect is proposed, which is one of the factors contributing to the application of the Casson fluid flow problem past a sphere. MHD refers to the study of fluid motion influenced by magnetic and electric fields, with its name reflecting magnetic fields ("magneto"), fluids ("hydro"), and motion ("dynamics"). It operates under Faraday's law of electromagnetic induction [14]. MHD is known as hydromagnetic that produces the Lorentz force in the electrically conducting fluid. This effect has significant applications in various fields, including thermal management systems, heat exchangers, solar energy harvesting, and electronic cooling [22]. According to Alkasasbeh [4], magnetohydrodynamic (MHD) analysis plays a vital role in interpreting various natural and industrial processes, such as the formation of stars, mixing of alloy elements, electrolysis, MHD energy conversion, and magnetic filtration and separation techniques. Singh and Kalathi [13] declared that it is important to study MHD Casson flow past a sphere,

which benefits in improving the efficiency of compression molding processes and optimizing rod functionality. Several applications of MHD Casson fluid flow past a sphere have been identified in recent years. These include its relevance in metallurgy and drilling operations, where precise control of fluid dynamics is crucial for ensuring efficiency and safety [12]; in biomedical applications such as blood flow, where its unique properties affect fluid behavior in complex geometries [18]; and in the design of heat exchangers and biomedical devices to improve the efficiency of various industrial processes [27]. Thus, the MHD Casson flow past a sphere has been widely investigated due to its broad practical relevance, including studies on rotating spheres [25, 3] and rigid spheres [2, 24].

In addition to magnetic effects, mixed convection heat transfer is another critical factor that significantly influences the behavior of Casson fluid flow past a sphere. Mixed convection arises from the combined effects of free (buoyancy-driven) and forced (externally applied) convection, making it essential for accurately modeling practical fluid flow systems. Numerous scientific and technological fields, including centrifugal blood pumps, rotary gears, fiber coating, polymer deposition and other devices, depend on mixed convection flows over a sphere [29]. As a result, some studies have investigated heat transmission by MHD mixed convection past a sphere. For the case of a rotating sphere, Mahdy et al. [19] and Ali et al. [3] numerically used the fourth-order Runge-Kutta Fehlberg method and Galerkin-based finite elements, respectively, to address the problem in MHD Casson mixed convection. Their results indicated that increasing the Casson parameter leads to a rise in fluid velocity and a reduction in temperature. Similarly, Alwawi et al. [6] observed that an increase in the mixed convection parameter results in a rise in velocity and a reduction in temperature. Sahaya et al. [26] and El-Zahar et al. [10] reported that increasing the MHD parameter with time leads to a higher heat transfer rate. Furthermore, Singla et al. [29] suggested that an increase in the Casson parameter enhances the heat transfer in a fluid flow. However, all of these studies have focused exclusively on fluid flow past a rotating sphere. To date, there has been no research addressing the flow of MHD Casson fluid with mixed convection heat transfer around a rigid (non-rotating) sphere, leaving a gap in the current literature.

Based on the mentioned literature, many studies have investigated steady and unsteady magnetohydrodynamic (MHD) flows, with particular emphasis on heat transfer in Newtonian and non-Newtonian fluids. The Casson fluid model, widely used to simulate blood flow, has been applied to understand arterial behavior and drug delivery systems. Although mixed convection in MHD Casson flow past spheres has been studied, most research has focused on rotating spheres, and the effects of flow reversal in unsteady MHD Casson flow past a rigid sphere remain largely unexplored. Recognizing this gap, the present study is driven by the need to better understand and mitigate the effects of flow reversal in such systems, particularly near stagnation points. The study employs the Keller box method to solve the governing boundary layer equations, providing accurate and stable solutions for nonlinear unsteady problems [20]. The findings offer new insights into the interplay between magnetic fields, non-Newtonian fluid effects, and flow reversal dynamics, with significant implications for biomedical and engineering systems, particularly in improving blood flow management and drug delivery.

Nomenclature:

M	Magnetic parameter
Pr	Prandtl number
Re	Reynolds number
r	non-dimensional radial axis of the sphere
u, v	non-dimensional velocity components for $x-$axis and $y-$axis
$u_e(x)$	non-dimensional external velocity
μ_B	Plastic dynamic viscosity of non-Newtonian fluid
π_c	Critical value
ρ_y	Yield stress of the fluid
ν	Kinematic viscosity

2 Mathematical Formulation

Consider MHD Casson fluid flow past an impermeable solid sphere in the direction of $\bar{x}-$axis and $\bar{y}-$axis where the velocity components $\bar{u}$ and $\bar{v}$ respectively in two-dimensional unsteady cases. Free stream velocity U_∞ of the fluid flow is decided be impulsively started at time $\bar{t} = 0$ in the upward direction passing a sphere with radius a and opposite with the gravitational force, $\bar{g}$. The applied magnetic field B_o is set to be perpendicular to the direction of the fluid flow and the induced magnetic field is ignored in this study. The temperature of the fluid flow is T_∞ and the temperature of the surface of the sphere is T_w. The boundary layer flow gives rise at the forward stagnation point $(\bar{x} = 0°)$ to rear stagnation point $(\bar{x} = 180°)$ as the time increases and the fluid flow starts impulsively.

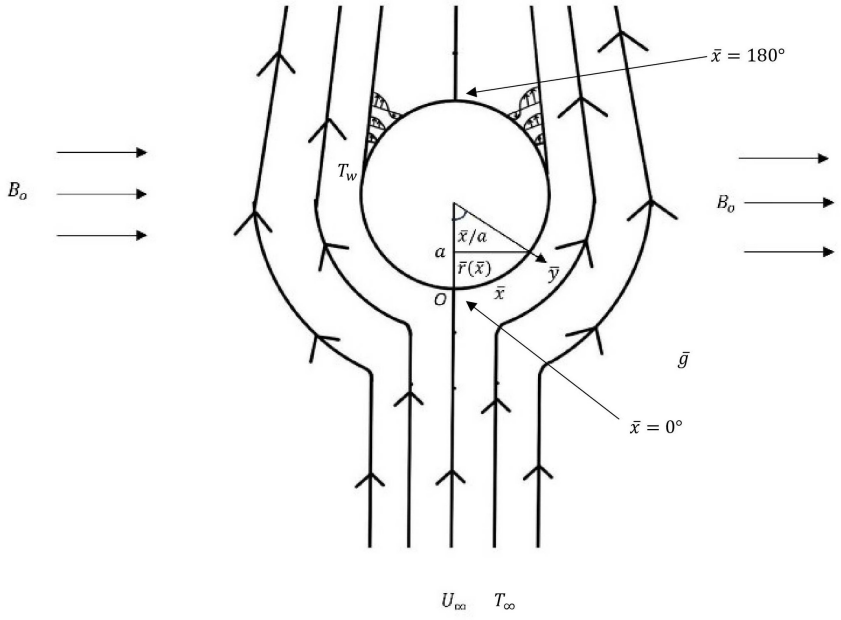

Figure 1: Coordinate system of the fluid flow.

The mathematical equations in dimensional form for the mentioned problem are as below,

$$\frac{\partial(\bar{r}\bar{u})}{\partial\bar{x}}+\frac{\partial(\bar{r}\bar{v})}{\partial\bar{y}}=0, \tag{1}$$

$$\frac{\partial\bar{u}}{\partial\bar{t}}+\bar{u}\frac{\partial\bar{u}}{\partial\bar{x}}+\bar{v}\frac{\partial\bar{u}}{\partial\bar{y}}=-\frac{1}{\rho}\frac{d\bar{p}}{d\bar{x}}+\frac{\mu}{\rho}\left(1+\frac{1}{\beta}\right)\left(\frac{\partial^2\bar{u}}{\partial\bar{x}^2}+\frac{\partial^2\bar{u}}{\partial\bar{y}^2}\right)-\frac{\sigma B_o\bar{u}}{\rho}+\alpha\bar{T}\sin\bar{x}, \tag{2}$$

$$\frac{\partial\bar{T}}{\partial\bar{t}}+\bar{u}\frac{\partial\bar{T}}{\partial\bar{x}}+\bar{v}\frac{\partial\bar{T}}{\partial\bar{y}}=\frac{c}{\rho c_f}\left(\frac{\partial^2\bar{u}}{\partial\bar{x}^2}+\frac{\partial^2\bar{u}}{\partial\bar{y}^2}\right), \tag{3}$$

associated with,

$$\begin{aligned}
&\bar{t}<0:\bar{u}=\bar{v}=0, && \bar{T}=T_\infty, && \forall\bar{x},\bar{y},\\
&\bar{t}\geq 0:\bar{u}=\bar{v}=0, && \bar{T}=T_w, && \bar{y}=0,\\
&\bar{t}\geq 0:\bar{u}_e(\bar{x})=U_w, && \bar{T}=T_\infty, && \bar{y}\to\infty,
\end{aligned} \tag{4}$$

where $\bar{r}$ is the dimensional radial axis of the sphere, $\bar{T}$ is the dimensional temperature, c is the thermal conductivity, c_f is the specific heat of the fluid, ρ is the density, μ is the dynamic viscosity, β is the Casson parameter, σ is the electric conductivity and α is the mixed convective parameter. According to Jefri and Ali [15], the stream velocity for the sphere is defined as,

$$\frac{\bar{u}_e(\bar{x})}{2}+p=\text{constant}, \tag{5}$$

where

$$\bar{u}_e(\bar{x})=\frac{3}{2}\sin\bar{x}. \tag{6}$$

Outside the boundary layer, Mohammad et al. [21] assumed that the temperature is neglected. Thus, the dimensional pressure of the fluid flow can be replaced by,

$$-\frac{d\bar{p}}{d\bar{x}}=\bar{u}_e\frac{d\bar{u}_e}{d\bar{x}}+M\bar{u}_e. \tag{7}$$

Next, the following non-dimensional variables suggested for the governing equations are as follows,

$$\begin{aligned}
&t=U_\infty\frac{\bar{t}}{a}, && x=\frac{\bar{x}}{a}, && y=\mathrm{Re}^{1/2}\frac{\bar{y}}{a}, && u=\frac{\bar{u}}{U_\infty},\\
&v=\mathrm{Re}^{1/2}\frac{\bar{v}}{U_\infty}, && p=\frac{\bar{p}}{\rho U_\infty^2}, && r=\frac{\bar{r}(\bar{x})}{a}, && T=\frac{\bar{T}-T_\infty}{\bar{T}_w-T_\infty},
\end{aligned} \tag{8}$$

where

$$\beta=\frac{\mu_b\sqrt{2\pi_c}}{\rho_y}, \qquad M=\frac{a\sigma B_o^2}{\rho U_\infty}, \qquad \mathrm{Pr}=\frac{\upsilon\rho c_f}{c}, \qquad \upsilon=\frac{\mu}{\rho}. \tag{9}$$

Therefore, (1)−(4) become,

$$\frac{\partial(ru)}{\partial x}+\frac{\partial(rv)}{\partial y}=0, \tag{10}$$

$$\frac{\partial u}{\partial t}+u\frac{\partial u}{\partial x}+v\frac{\partial u}{\partial y}=u_e\frac{du_e}{dx}+\frac{\mu}{\rho}\left(1+\frac{1}{\beta}\right)\left(\frac{\partial^2u}{\partial y^2}\right)+M(u_e-u)+\alpha T\sin(x), \tag{11}$$

$$\frac{\partial T}{\partial t}+u\frac{\partial T}{\partial x}+v\frac{\partial T}{\partial y}=\frac{1}{\mathrm{Pr}}\frac{\partial^2u}{\partial y^2}, \tag{12}$$

subject to

$$\begin{aligned} t<0: u=v=0, &\quad T=T_\infty, &\quad \forall x,y,\\ t\geq 0: u=v=0, &\quad T=T_w, &\quad y=0,\\ t\geq 0: u_e(x)=U_w, &\quad T=T_\infty, &\quad y\to\infty. \end{aligned} \tag{13}$$

Following Cebeci [9], small ($t<t^*$) and large ($t>t^*$) time case is introduced to reduce the singularity at a specific time. This study considered forward ($x=0°$) and rear ($x=180°$) stagnation point at the surface of the sphere. Thus, the term $\frac{du_e}{dx}$ is replaced by $\frac{3}{2}\lambda$ where $\lambda=1$ for forward stagnation while $\lambda=-1$ is for the rear stagnation point. Equations (10)−(13) are transformed to the stream function where,

For small time case:

$$\eta=\frac{y}{t^{1/2}}, \psi=t^{1/2}u_e(x)r(x)f(x,\eta,t), T=s(x,\eta,t). \tag{14}$$

For large time case:

$$\eta=Y, \psi=u_e(x)r(x)F(x,Y,t), T=S(x,Y,t). \tag{15}$$

Thus, the equations for the small time case become,

$$\left(1+\frac{1}{\beta}\right)f'''+\frac{\eta}{2}f''+\frac{3}{2}\lambda t(1-(f')^2+ff'')+Mt(1-f')+\frac{2}{3}\alpha ts=t\frac{\partial f'}{\partial t}, \tag{16}$$

$$s''+\mathrm{Pr}\frac{\eta}{2}s'+\mathrm{Pr}t\frac{3}{2}\lambda fs'=\mathrm{Pr}t\frac{\partial s'}{\partial t}, \tag{17}$$

with (13) are written correspondingly as,

$$\begin{aligned} t<0: f=f'=0, &\quad s=0, &\quad \forall x,\eta,\\ t\geq 0: f=f'=0, &\quad s=1, &\quad \eta=0,\\ t\geq 0: f'=1, &\quad s=0, &\quad \eta\to\infty. \end{aligned} \tag{18}$$

The equations for large time case are as follows,

$$\left(1+\frac{1}{\beta}\right)F'''+\frac{3}{2}\lambda(1-(F')^2+FF'')+M(1-F')+\frac{2}{3}\alpha S=\frac{\partial F'}{\partial t}, \tag{19}$$

$$S''+\mathrm{Pr}\frac{3}{2}\lambda FS'=\mathrm{Pr}\frac{\partial S'}{\partial t}, \tag{20}$$

with boundary conditions,

$$\begin{aligned} F=F'=0, &\quad S=1, &\quad Y=0,\\ F'=1, S=0 &\quad Y\to\infty. \end{aligned} \tag{21}$$

According to Kasim et al. [17], the exact solution that can be obtained from (16)−(18) when $t=0$

are used to be the starting conditions and the validating benchmark for this study, where,

$$f = \sqrt{\frac{\beta+1}{\beta}}\left[\eta \text{erf}\left(\frac{\eta}{2}\sqrt{\frac{\beta}{\beta+1}}\right)\right] + \frac{2}{\sqrt{\pi}}\left[\exp\left[\frac{-\beta\eta^2}{4(\beta+1)}\right] - 1\right], \tag{22}$$

$$f' = \sqrt{\frac{\beta+1}{\beta}}\left[\text{erf}\left(\frac{\eta}{2}\sqrt{\frac{\beta}{\beta+1}}\right)\right], \tag{23}$$

$$f'' = \frac{1}{\pi}\exp\left[\frac{-\beta\eta^2}{4(\beta+1)}\right], \tag{24}$$

$$s = 1 - \text{erf}\left(\frac{\sqrt{\text{Pr}}}{2}\eta\right), \tag{25}$$

$$s' = -\sqrt{\frac{\text{Pr}}{\pi}}\exp\left(-\frac{\text{Pr}}{4}\eta^2\right). \tag{26}$$

3 Numerical Analysis

The Keller box method was selected for solving unsteady boundary layer flow problems because of its simplicity and efficiency, especially when the exact solution is only known at $t = 0$. It is well-suited for handling complex, non-linear boundary layer equations and is easy to be implemented in MATLAB. The MATLAB code runs in under one minute on an Intel i5 processor, demonstrating high computational efficiency. Additionally, since MATLAB is widely accessible to many users at no extra cost, the overall expense of the numerical routine is minimal. These advantages-fast computation, ease of implementation, low cost, and effective performance-make the Keller box method more efficient than other approaches like the Finite Element method which often demand more computational power [20].

The equations (16)−(21) is solved by using the Keller Box method with the aid of starting conditions (22)−(26). Thus, higher-order partial differential equations (PDE) are reduced to the first order PDE. The reduced equations are then discretized by the finite difference method and linearized by Newton's approach. The results for velocity and temperature are analyzed graphically in MATLAB. The convergence of the numerical calculation is set to be less than 10^{-6} to achieve a stable result. By using $\triangle\eta = 0.1$ and $\triangle t = 0.05$, the results are obtained in tabular form and validated with exact results in (24) and (26) as displayed in Tables 1−3. The numerical findings indicate an excellent agreement with the exact solution.

Table 1: Validation of $f''(0)$ for various values of β when $t = 0$.

β	Exact equation (24)	Present (numerical solution)	Residual squared error
0.5	0.3257	0.3258	1×10^{-8}
1.0	0.3989	0.3990	1×10^{-8}
2.0	0.4607	0.4608	1×10^{-8}
5.0	0.5150	0.5152	4×10^{-8}

Table 2: Validation of $s'(0)$ for various values of Pr when $t = 0$.

Pr	Exact equation (26)	Present (numerical solution)	Residual squared error
0.7	-0.4720	-0.4721	1.000×10^{-8}
1.0	-0.5642	-0.5544	9.604×10^{-5}
7.0	-1.4927	-1.4960	1.089×10^{-5}

Table 3: Validation of $f''(\eta)$ and $s'(\eta)$ for different values of η when $t = 0, \beta = 1, \mathrm{Pr} = 0.7$.

η	$f''(\eta)$			$s'(\eta)$		
	Exact equation (24)	Present (numerical solution)	Residual squared error	Exact equation (26)	Present (numerical solution)	Residual squared error
0.0	0.3989	0.3990	1.00×10^{-8}	-0.4720	-0.4721	1×10^{-8}
0.5	0.3748	0.3867	1.42×10^{-4}	-0.4518	-0.4519	1×10^{-8}
1.0	0.3521	0.3521	0.0000	-0.3963	-0.3963	0.0000
1.5	0.3307	0.3307	0.0000	-0.3184	-0.3185	4×10^{-8}

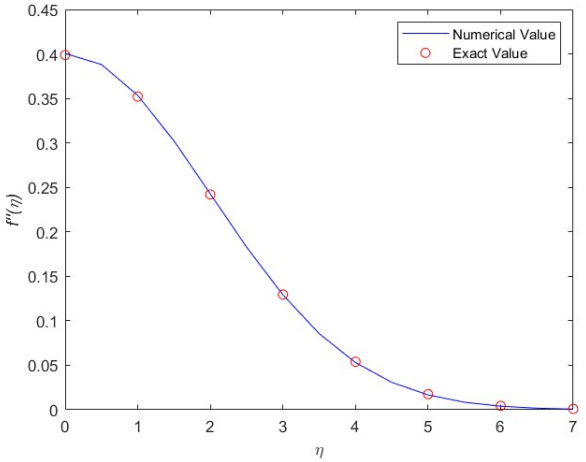

Figure 2: Comparison of $f''(\eta)$ between numerical and exact value.

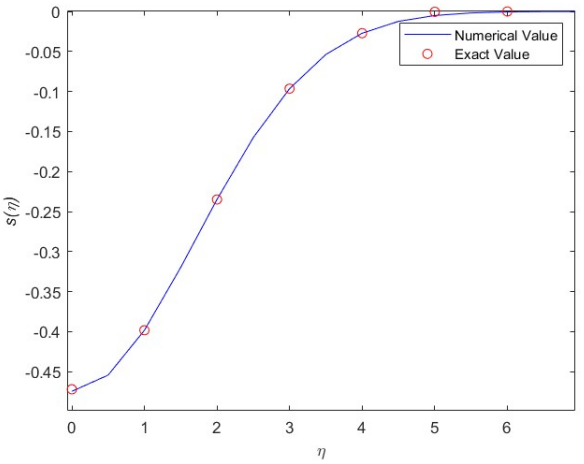

Figure 3: Comparison of $s'(\eta)$ between numerical and exact value.

4 Results and Discussion

The range of physical parameters of this study was carefully selected to explore the effects of different fluid properties and flow conditions on the unsteady MHD heat transfer by mixed convection in a Casson fluid flow past a sphere. The chosen range of M and β values effectively highlight the distinct trend of flow reversal in response to increasing magnetic field strength and Casson parameter. The Prandtl numbers 0.7, 1, and 7 correspond to the thermal properties of various fluids representing air, a standard reference fluid and water, respectively. For illustration purposes, it is adequate to choose the value of M from 0 to 5 and β excluding 0, to demonstrate the trends of the selected profiles, as there are no specific limitations in this study.

In Figure 4, the velocity profile of the Casson fluid past a sphere at time $t = 1.5$ is plotted as $\alpha = 0$ and $\beta = 1$ with various values of M . Figure 4(a) indicates the velocity of fluid flow at $x = 0°$, while for $x = 180°$ is as in Figure 4(b). As M increases, the velocity profile observed in both stagnation points increases, and the thickness of momentum boundary layer decreases. As shown in Figure 4(b), there exist negative values in the velocity profile for the case $M = 0$ up to 1. This shows that there exists a flow reversal of fluid flow at $x = 180°$ for certain values of M. The increase in M cause a reduction of the flow reversal. Overall, the velocity for both stagnation points increased due to the Lorentz force that enhanced the momentum of the fluid flow.

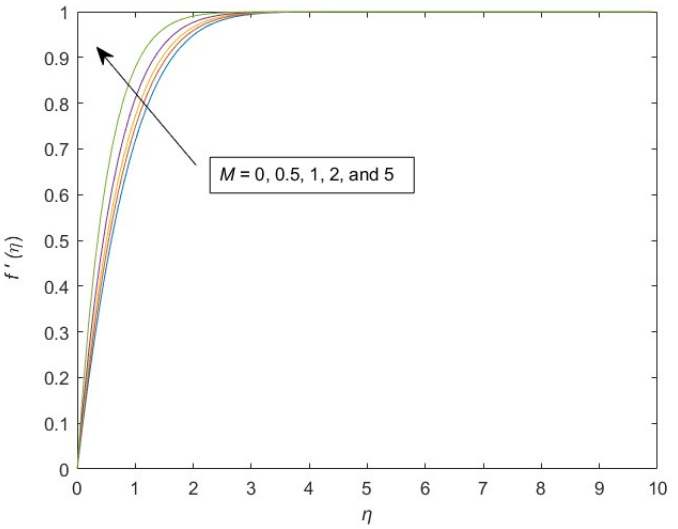

(a)

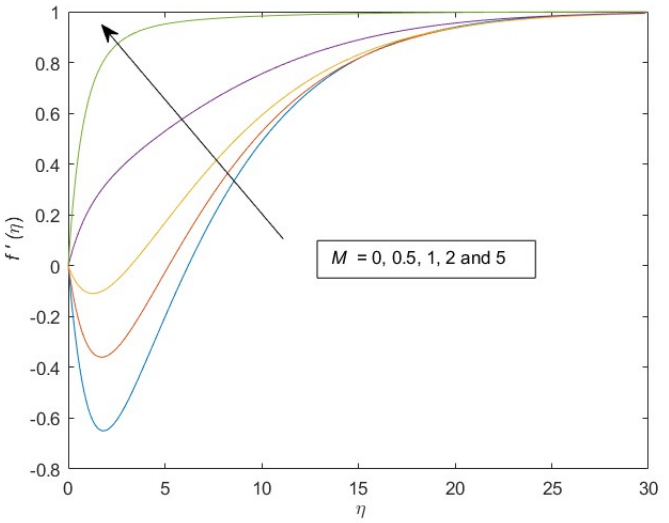

(b)

Figure 4: Velocity profiles at time $t = 1.5$ in variation values of M at (a) $x = 0^\circ$ and (b) $x = 180^\circ$.

The temperature profiles at the stagnation points for various M values are shown in Figure 5. In Figure 5(a), $s(\eta)$ decreases as the M values rises at the front of the sphere. This is due to the reduction of the thermal boundary layer. Therefore, the heat transfer from the sphere to the fluid is slow, and the cooling effect occurs at $x = 0^\circ$. On the other hand, the thermal boundary layer at $x = 180^\circ$ increases due to the rise of M value. Consequently, the heat transfer rate is quick and results to an increase in the temperature of the fluid flow. Thus, the cooling effect occurs at $x = 0^\circ$, while the heating effect occurs at $x = 180^\circ$.

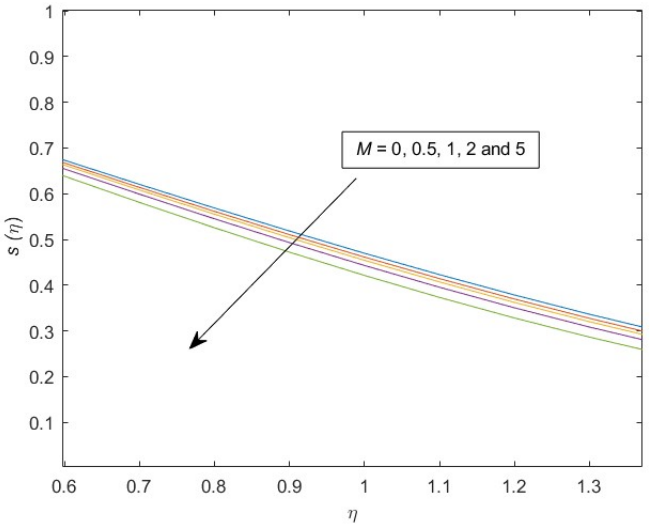

(a)

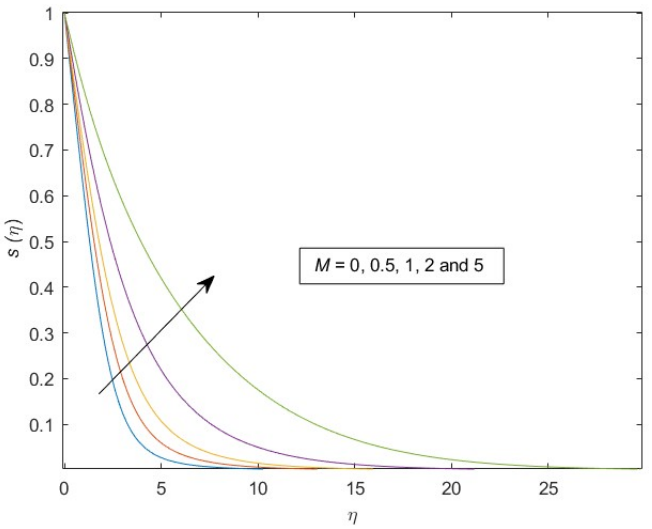

(b)

Figure 5: Temperature profiles at time $t = 1.5$ in variation values of M at (a) $x = 0^\circ$ and (b) $x = 180^\circ$.

Based on Figure 6, the Pr values of 0.7(air) and 7(water) are chosen in this study. The thermal boundary layer is higher if Pr less than 1 and lower at Pr greater than 1. A greater thermal boundary layer increases the rate of heat convection. From Figure 6, the fluid temperature decreases rapidly at $x = 0^\circ$ compared to at $x = 180^\circ$ as the Pr value increase. The thermal boundary layer $\text{Pr} = 0.7$ is higher than $\text{Pr} = 7$. This implies that the rate of heat transfer for $\text{Pr} = 0.7$ is higher than $\text{Pr} = 7$. Therefore, as Pr value increases from 0.7 to 7, the heat transfer rate gradually decreases. That is why the temperature of the fluid decreases as Pr increase.

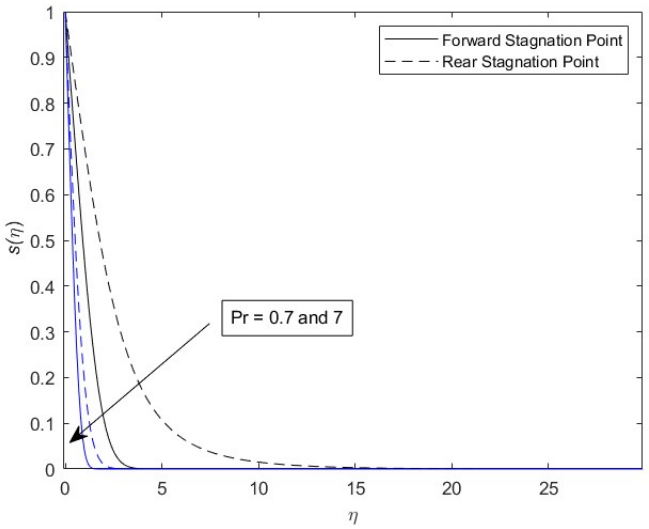

Figure 6: Temperature profile of the Prandtl number at (a) $x = 0°$ and (b) $x = 180°$.

Figure 7 shows different values of the Casson parameter, β at forward and rear stagnation points. Based on Figure 7(a), the velocity increases with increasing β which implies that the Casson parameter increases the momentum of the fluid at the point $x = 0°$. At the point $x = 180°$, the velocity profile decreases at a small value of η and increases rapidly approaching 1 as shown in Figure 7(b). The flow reversal at the rear stagnation point remains as the β value increases. This means that the increase of the Casson parameter does not significantly affect the reduction of flow reversal.

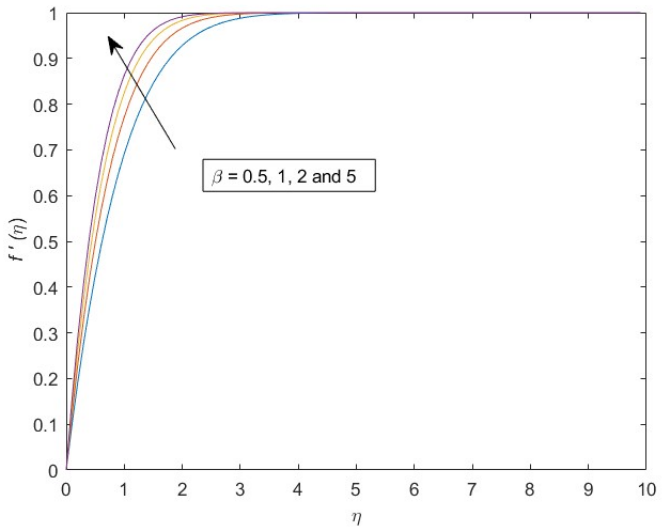

(a)

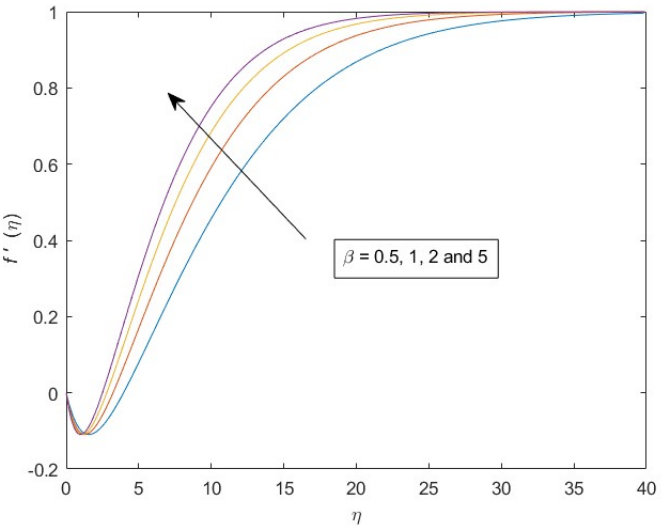

(b)

Figure 7: Velocity profiles at time $t = 1.5$ in variation values of β at (a) $x = 0^\circ$ and (b) $x = 180^\circ$.

The energy profiles in the variation of the Casson parameter, β are shown in Figure 8. The cooling effect and heat effect are seen in both stagnation points, respectively. An increase in M and β as in Figure 5(b) and Figure 8(b) indicate the heating effect, while Figure 5(b) and Figure 8(b) indicate the cooling effect. However, the increase of M is more significant than β.

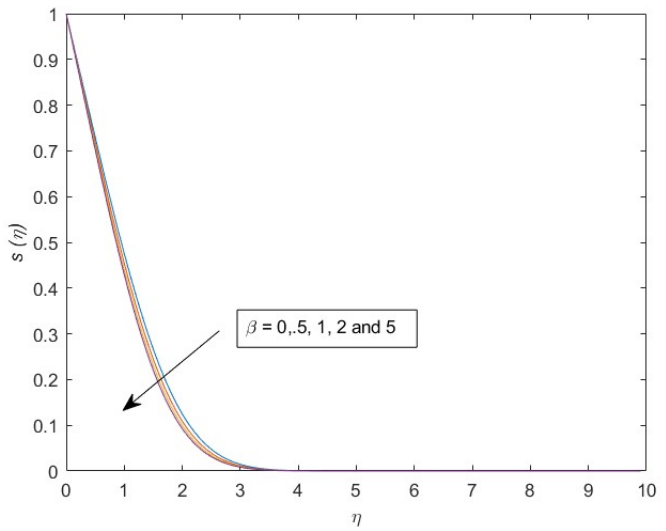

(a)

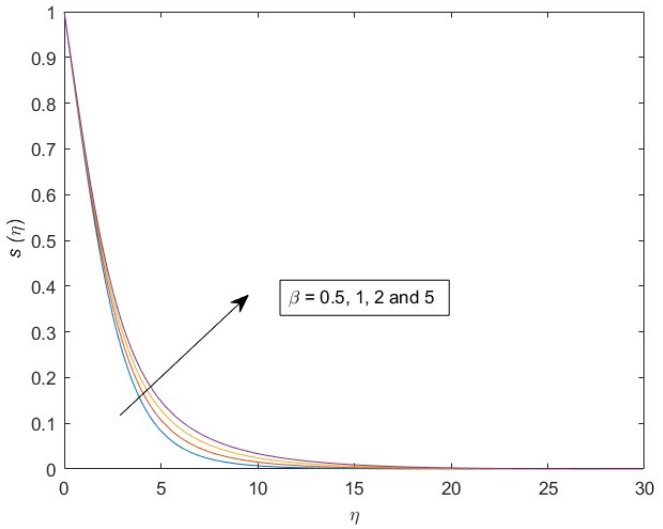

(b)

Figure 8: Temperature profiles at time $t = 1.5$ in variation values of β at (a) $x = 0^\circ$ and (b) $x = 180^\circ$.

Since this study considers mixed convection heat transfer, the assisting flow $(\lambda = 1)$ and opposing flow $(\lambda = -1)$ need to be analysed. The assisting flow refers to the buoyancy force which is more dominant in the fluid flow, while the opposing flow indicates the external force is dominant. Based on Figure 9(a), the increasing pattern is observed in $\lambda = 1$ and $\lambda = -1$ as M increase. But then, the rapid increase of the velocity profile at $x = 0^\circ$ when the M value increases from 1 to 5. Physically, the existence of the Lorentz force generated by the magnetic field resists the fluid flow at $M = 0$. Then, the M value increases, the Lorentz force starts to increase the velocity of the fluid flow. At $x = 180^\circ$, the flow reversal of opposing flow is higher than assisting flow at η between 0 to 5 as shown in Figure 9(b). Thus, the velocity of $\lambda = -1$ is lower than for $\lambda = 1$ in the range of η between 0 and 5. From the value of η greater than 5, the velocity profile of the opposing case increases rapidly compared to the assisting flow. In Figure 9(a), the large value of M is considered due to the significant difference in the velocity profile. Besides, the small increase of M is chosen due to the small amount of M value could reduce the flow reversal at $x = 180^\circ$.

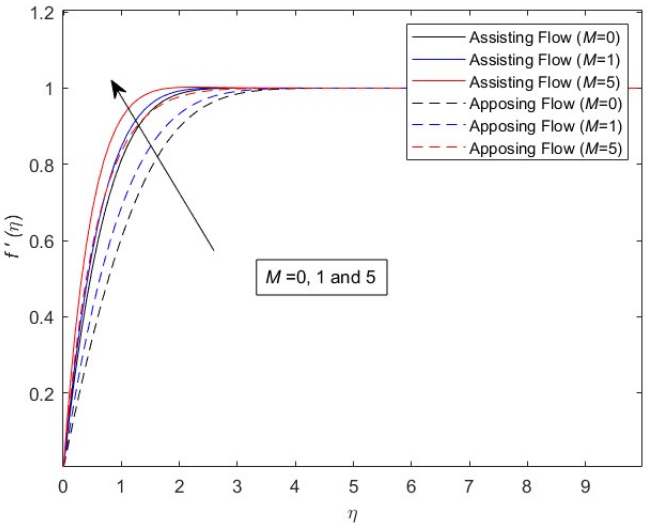

(a)

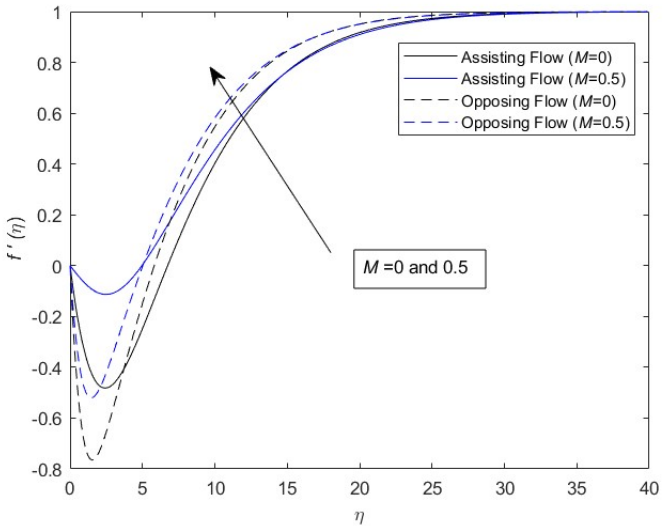

(b)

Figure 9: Velocity profiles at time $t = 1.5$ in variation values of M at (a) $x = 0°$ and (b) $x = 180°$.

Figure 10(a) shows that the temperature of the opposing flow decreases rapidly compared to the assisting flow as M value increases from 1 to 5. At $x = 0°$, temperature decreases more rapidly in the opposing flow than in the assisting flow compared to at $x = 180°$.

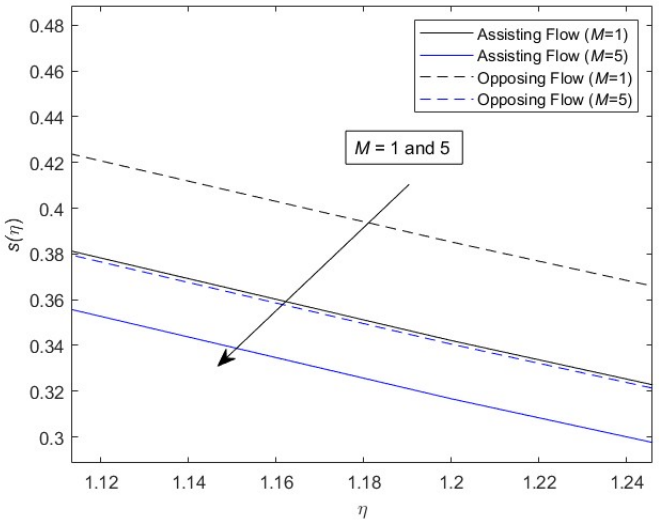

(a)

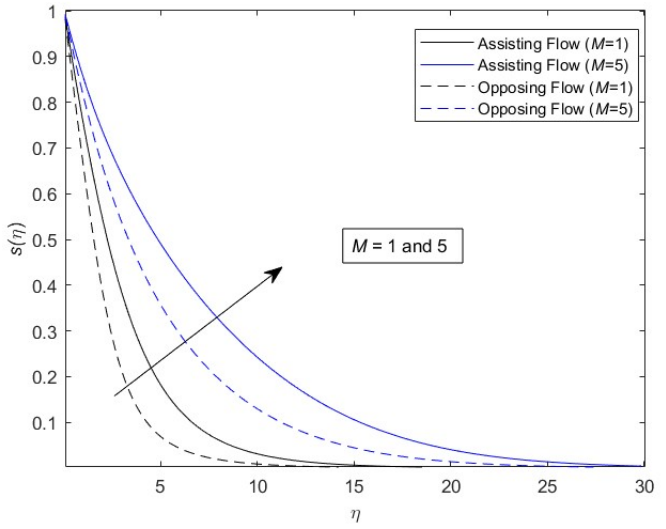

(b)

Figure 10: Temperature profiles at time $t = 1.5$ in variation values of M at (a) $x = 0^\circ$ and (b) $x = 180^\circ$.

5 Conclusions

The novelty of this study lies in the investigation of unsteady MHD Casson flow past a stationary sphere, which provides new insights into the dynamics of flow reversal. Several assumptions have been made to simplify the complex physical problem. The fluid is considered as an incompressible Casson fluid, which is an idealized model and may not capture all the complexities of real non-Newtonian fluids. The geometry of the domain is assumed to be a perfect sphere, which is helpful in mathematical modeling but may differ from irregular shapes encountered in prac-

tical applications, such as biological systems. The influence of the magnetic field is assumed to be uniform and constant, ignoring spatial or temporal variations that may occur in real-world scenarios. Additionally, the effect of nanofluids is not considered in this analysis. Buongiorno's model, which takes into account the dynamics of nanoparticles such as Brownian motion and thermophoresis, was specifically designed for nanofluid behavior and is therefore not applicable in this study. This is primarily because the current investigation focuses on a classical Casson fluid without any addition of nanoparticles, thus maintaining a simpler and more tractable model for the fundamental analysis. The inclusion of nanofluid effects would significantly complicate the governing equations and boundary conditions, requiring additional parameters and assumptions that are beyond the scope of this work. Moreover, nondimensional variables are employed throughout the analysis to eliminate physical units. This process of nondimensionalization not only simplifies the mathematical formulation, but also enhances the generality and scalability of the results, making the computations more efficient and the findings are easier to be interpreted across different fluid systems. These assumptions may limit the direct applicability of the results to more complex real-world problems, but they allow for a clearer understanding of the fundamental behavior of unsteady MHD mixed convection flow in Casson fluids. Future studies could extend this work by incorporating more realistic boundary conditions, variable magnetic fields, and more complex fluid models.

Furthermore, this study is theoretical and numerical, focusing on the development and analysis of an unsteady MHD mixed convection model for Casson fluid flow past a sphere. Although no experiments were conducted, the numerical results showed excellent agreement with benchmark solutions from the literature, confirming the reliability of the model. Future work may include experimental validation to strengthen its applicability in engineering and biomedical contexts. The momentum equation is used in its standard form based on the Navier-Stokes equations to capture essential flow phenomena, including viscosity, pressure, and the Lorentz force from the magnetic field. The MHD term is crucial for modeling the interaction between the fluid and magnetic field, which significantly influences flow behavior in various applications. The energy equation incorporates convective heat transfer and magnetic field effects on temperature, assuming constant thermal conductivity and no radiative heat transfer, which is common in engineering systems. The Prandtl number is also included to account for thermal diffusivity and ensure a more accurate depiction of heat transfer.

To sum up, the effects of MHD, Casson, and mixed convection parameters on flow reversal at stagnation points are investigated. The results show that the magnetic field significantly reduces flow reversal at the rear stagnation point, which is important for controlling blood flow in medical applications such as drug delivery and vascular treatments. While the Casson parameter has a smaller impact on flow reversal, it still affects the overall flow behavior. Additionally, the fluid exhibits a cooling effect at the front stagnation point and a heating effect at the rear. These findings offer valuable insights that are of great relevance for both biological and industrial applications. In biological systems, such as blood circulation, understanding the interaction of blood (modeled as a Casson fluid) with magnetic fields can lead to advances in medical technologies like drug delivery and artificial organs. In industrial applications, such as fluidized beds or catalytic reactors, studying the behavior of fluids around rigid spherical particles contributes to a better understanding of heat transfer, particle dynamics, leading to more efficient system design.

Acknowledgement The authors are thankful to UTM Nexus for their financial support.

Conflicts of Interest The authors declare no conflict of interest.

References

[1] A. Al-hanaya, Z. Z. Rashed & S. E. Ahmed (2024). MHD Casson flow over a solid sphere surrounded by porous material in the presence of Stefan blowing and slip conditions. *Alexandria Engineering Journal*, *103*, 402–412. https://doi.org/10.1016/j.aej.2024.07.018.

[2] A. R. Ali, K. Rafique, M. Imtiaz, R. Jan, H. Alotaibi & I. Mekawy (2024). Exploring magnetic and thermal effects on MHD bio-viscosity flow at the lower stagnation point of a solid sphere using Keller box technique. *Partial Differential Equations in Applied Mathematics*, *9*, Article ID: 100601. https://doi.org/10.1016/j.padiff.2023.100601.

[3] B. Ali, A. Shafiq, A. Manan, A. Wakif & S. Hussain (2022). Bioconvection: Significance of mixed convection and MHD on dynamics of Casson nanofluid in the stagnation point of rotating sphere via finite element simulation. *Mathematics and Computers in Simulation*, *194*, 254–268. https://doi.org/10.1016/j.matcom.2021.11.019.

[4] H. T. Alkasasbeh (2023). Numerical investigation of MHD Carreau hybrid nanofluid flow over a stretching sheet in a porous medium with viscosity variations and heat transport. *Journal of Computational Applied Mechanics*, *54*(3), 410–424. https://doi.org/10.22059/JCAMECH.2023.364255.861.

[5] H. T. Alkasasbeh (2024). Exploring three-dimensional MHD Maxwell hybrid nanofluid flow: A computational study on a stretching sheet. *Journal of Computational Applied Mechanics*, *55*(1), 77–91. https://doi.org/10.22059/jcamech.2024.369138.916.

[6] F. A. Alwawi, H. T. Alkasasbeh, A. M. Rashad & R. Idris (2020). A numerical approach for the heat transfer flow of carboxymethyl cellulose-water based Casson nanofluid from a solid sphere generated by mixed convection under the influence of Lorentz force. *Mathematics*, *8*(7), Article ID: 1094. https://doi.org/10.3390/math8071094.

[7] A. Amin, S. Munir & U. Farooq (2024). Flow dynamics and convective transport analysis of two-layered dissipative Casson hybrid nanofluid flow in a vertical channel. *Proceedings of the Institution of Mechanical Engineers, Part C: Journal of Mechanical Engineering Science*, *238*(2), 395–404. https://doi.org/10.1177/09544062231170753.

[8] W. F. W. Azmi, A. Q. Mohamad, L. Y. Jiann & S. Shafie (2024). Mathematical fractional analysis on blood Casson fluid in slip and small arteries with the cholesterol porosity effect. *Malaysian Journal of Mathematical Sciences*, *18*(4), 755–774. https://doi.org/10.47836/mjms.18.4.05.

[9] T. Cebeci (1979). The laminar boundary layer on a circular cylinder started impulsively from rest. *Journal of Computational Physics*, *31*(2), 153–172. https://doi.org/10.1016/0021-9991(79)90068-8.

[10] E. R. El-Zahar, A. E. N. Mahdy, A. M. Rashad, W. Saad & L. F. Seddek (2021). Unsteady MHD mixed convection flow of non-Newtonian Casson hybrid nanofluid in the stagnation zone of sphere spinning impulsively. *Fluids*, *6*(6), Article ID: 197. https://doi.org/10.3390/fluids6060197.

[11] A. Fayyaz, Z. Abbas & M. Y. Rafiq (2024). Exploration of the dynamics of heated non-Newtonian Casson fluid within an annular region of eccentric cylinders subject to peristaltic motion. *Proceedings of the Institution of Mechanical Engineers, Part E: Journal of Process Mechanical Engineering*, pp. Article ID: 09544089241279215. https://doi.org/10.1177/09544089241279215.

[12] S. A. Gaffar, K. Ur-Rehman, P. R. Reddy, V. R. Prasad & B. M. H. Khan (2019). Powell–Eyring fluid flow towards an isothermal sphere in a non-Darcy porous medium. *Canadian Journal of Physics*, *97*(10), 1039–1048. https://doi.org/10.1139/cjp-2018-0835.

[13] K. Gnanaprasanna & A. K. Singh (2023). A numerical approach of forced convective MHD Casson hybrid nano fluid flows exposed to Joule heating and viscous dissipation over diverging channel. *Journal of Porous Media*, *27*(4), 1–21. https://doi.org/10.1615/JPorMedia.2023047328.

[14] A. Hyder, I. Jiann L Y Khan & S. Shafie (2024). Thermal behavior of MHD stagnation ternary nanofluid over a melting surface with Joule heating. *Malaysian Journal of Mathematical Sciences*, *19*(2), 361–381. https://doi.org/10.47836/mjms.19.2.01.

[15] N. N. N. Jefri & A. Ali (2024). Unsteady dusty MHD boundary layer flow past a sphere. In *ITM Web of Conferences*, volume 67 pp. Article ID: 01030. EDP Sciences. https://doi.org/10.1051/itmconf/20246701030.

[16] H. Jiang (2020). Separation angle for flow past a circular cylinder in the subcritical regime. *Physics of Fluids*, *32*(1), Article ID: 014106. https://doi.org/10.1063/1.5139479.

[17] A. R. M. Kasim, N. S. Arifin, N. A. N. Ariffin, M. Z. Salleh & M. I. Anwar (2020). Mathematical model of simultaneous flow between Casson fluid and dust particle over a vertical stretching sheet. *International Journal of Integrated Engineering*, *12*(3), 253–260.

[18] U. Khan, F. Mebarek-Oudina, A. Zaib, A. Ishak, S. Abu Bakar, E. S. M. Sherif & D. Baleanu (2022). An exact solution of a Casson fluid flow induced by dust particles with hybrid nanofluid over a stretching sheet subject to Lorentz forces. *Waves in Random and Complex Media*, *35*(5), 1–14. https://doi.org/10.1080/17455030.2022.2102689.

[19] A. Mahdy & S. E. Ahmed (2017). Unsteady MHD convective flow of non-Newtonian Casson fluid in the stagnation region of an impulsively rotating sphere. *Journal of Aerospace Engineering*, *30*(5), Article ID: 04017036. https://doi.org/10.1061/(ASCE)AS.1943-5525.0000700.

[20] M. K. A. Mohammad, H. R. Ong, S. K. Soid & H. T. Alkasasbeh (2025). Unsteady MHD mixed convection flow of water over a sphere with mass transfer. *Journal of Advanced Research in Numerical Heat Transfer*, *25*(1), 25–36. https://doi.org/10.37934/arnht.25.1.2536.

[21] N. F. Mohammad, A. R. M. Kasim, A. Ali & S. Shafie (2014). Separation times analysis of unsteady magnetohydrodynamics mixed convective flow past a sphere. In *AIP Conference Proceedings*, volume 1605 pp. 349–354. American Institute of Physics. https://doi.org/10.1063/1.4887614.

[22] S. Munir & Y. U. U. B. Turabi (2025). Impact of heated wavy wall and hybrid nanofluid on natural convection in a triangular enclosure with embedded cold cylinder under inclined magnetic field. *Arabian Journal for Science and Engineering*, *50*(6), 4007–4020. https://doi.org/10.1007/s13369-024-09450-3.

[23] G. Radha, N. Bhaskar Reddy & K. Gangadhar (2017). Slip flow of Casson fluid with variable thermo physical properties along exponentially stretching sheet under convective heating. *International Journal of Mechanics and Solids*, *12*(2), 235–256.

[24] K. Rafique, I. Khan & M. Bakouri (2025). Newtonian heating effects on Casson nanofluid flow at lower stagnation point of a solid sphere. *ZAMM-Journal of Applied Mathematics and Mechanics/Zeitschrift für Angewandte Mathematik und Mechanik*, *105*(1), Article ID: e202300873. https://doi.org/10.1002/zamm.202300873.

[25] A. Rehman, Z. Y. He, M. K. Wang, O. A. Almaghrabi, S. A. M. Alsallami & W. Khan (2022). Analytical study of time-dependent Mgnatohydrodynomics flow of hybrid nanofluid around a rotating sphere. *Waves in Random and Complex Media*, *2022*, 1–18. https://doi.org/10.1080/17455030.2022.2123967.

[26] A. Sahaya Jenifer, P. Saikrishnan & R. W. Lewis (2021). Unsteady MHD mixed convection flow of water over a sphere with mass transfer. *Journal of Applied and Computational Mechanics*, *7*(2), 935–943. https://doi.org/10.22055/jacm.2021.35920.2761.

[27] N. Sarma & A. Paul (2024). Engine oil blended Casson hybrid nanofluid flow along a uniformly heated curved surface with Arrhenius activation energy and suction: A computational study. *Hybrid Advances*, *5*, Article ID: 100161. https://doi.org/10.1016/j.hybadv.2024.100161.

[28] J. Singh, A. B. Vishalakshi, U. S. Mahabaleshwar & G. Bognar (2022). MHD Casson fluid flow with Navier's and second order slip due to a perforated stretching or shrinking sheet. *PLOS One*, *17*(11), Article ID: e0276870. https://doi.org/10.1371/journal.pone.0276870.

[29] T. Singla, B. Kumar & S. Sharma (2024). Mixed convective viscous dissipative flow of Casson hybrid nanofluid with variable thermal conductivity at the stagnation zone of a rotating sphere. *The Canadian Journal of Chemical Engineering*, *102*(11), 3879–3895. https://doi.org/10.1002/cjce.25352.

[30] A. Subbarao, V. R. Prasad, R. N. Bhaskar & B. O. Anwer (2015). Modelling laminar transport phenomena in a Casson rheological fluid from an isothermal sphere with partial slip. *Thermal Science*, *19*(5), 1507–1519. https://doi.org/10.2298/TSCI120828098S.

[31] A. Talaei & T. J. Garrett. An analytical solution to the Navier–Stokes equation for incompressible flow around a solid sphere. Preprint EarthArXiv 2020. https://doi.org/10.31223/osf.io/ktcde.

[32] Y. U. U. B. Turabi, S. Munir & A. Amin (2025). Numerical analysis of convective transport mechanisms in two-layer ternary $(TiO_2 - SiO_2 - Al_2O_3)$ Casson hybrid nanofluid flow in a vertical channel with heat generation effects. *Numerical Heat Transfer, Part A: Applications*, *86*(6), 1673–1687. https://doi.org/10.1080/10407782.2023.2281542.

[33] G. Vasanth Kumar & R. Mukherjee (2022). Study of separation lines and flow patterns in 3D boundary layer over sphere using experimental and numerical analysis. In *Fluid Mechanics and Fluid Power, Volume 6: Select Proceedings of FMFP 2022*, Lecture Notes in Mechanical Engineering pp. 273–286. Springer, Singapore. https://doi.org/10.1007/978-981-99-5755-2_29.

[34] D. R. Yanala, S. G. Bejawada & K. S. Nisar (2023). Influence of chemical reaction and heat generation/absorption on unsteady magneto Casson nanofluid flow past a non-linear stretching Riga plate with radiation. *Case Studies in Thermal Engineering*, *50*, Article ID: 103494. https://doi.org/10.1016/j.csite.2023.103494.

[35] S. Yuan, Y. Leng, A. Fouly, E. M. Awwad, U. Nazir & M. Sohail (2024). A study of four-phase fluid and thermal enhancement based on tetra-hybrid nanofluid considering temperature jump on a spinning sphere. *Case Studies in Thermal Engineering*, *58*, Article ID: 104353. https://doi.org/10.1016/j.csite.2024.104353.